Thermodynamic Roles of Basic Amino Acids in Statherin Recognition of Hydroxyapatite †

ARTICLE *in* BIOCHEMISTRY · APRIL 2007

Impact Factor: 3.02 · DOI: 10.1021/bi602345a · Source: PubMed

6 AUTHORS, INCLUDING:

Gil Goobes
Bar Ilan University
36 PUBLICATIONS **493** CITATIONS

SEE PROFILE

Thermodynamic Roles of Basic Amino Acids in Statherin Recognition of Hydroxyapatite†

Rivka Goobes,‡ Gil Goobes,§ Wendy J. Shaw,|| Gary P. Drobny,§ Charles T. Campbell,§ and Patrick S. Stayton*,‡

Departments of Bioengineering and Chemistry, University of Washington, Seattle, Washington 98195, and Pacific Northwest National Laboratory, Richland, Washington 99352

Received November 14, 2006; Revised Manuscript Received February 12, 2007

ABSTRACT: Salivary statherin is a highly acidic, 43 amino acid residue protein that functions as an inhibitor of primary and secondary crystallization of the biomineral hydroxyapatite. The acidic domain at the N-terminus was previously shown to be important in the binding of statherin to hydroxyapatite surfaces. This acidic segment is followed by a basic segment whose role is unclear. In this study, the role of the basic amino acids in the hydroxyapatite adsorption thermodynamics has been determined using isothermal titration calorimetry and equilibrium adsorption isotherm analysis. Single point mutations of the basic side chains to alanine lowered the binding affinity to the surface but did not perturb the maximal surface coverage and the adsorption enthalpy. The structural and dynamic properties of the single point mutants as characterized by solid-state NMR techniques were not altered either. Simultaneous replacement of all four basic amino acids with alanine lowered the adsorption equilibrium constant by 5-fold and the maximal surface coverage by nearly 2-fold. The initial exothermic phase of adsorption exhibited by native statherin is preserved in this mutant, along with the α-helical structure and the dynamic properties of the N-terminal domain. These results help to refine the two binding site model of statherin adsorption proposed earlier in our study of wild-type statherin (Goobes, R., Goobes, G., Campbell, C.T., and Stayton, P.S. (2006) *Biochemistry 45*, 5576−5586). The basic charges function to reduce protein−protein charge repulsion on the HAP surface, and in their absence, there is a considerable decrease in statherin packing density on the surface at binding saturation.

The primary role of the salivary protein statherin is to regulate the re-mineralization of hydroxyapatite (HAP[1]), the prevalent inorganic component of tooth enamel, by inhibiting both the nucleation and growth of HAP in the calcium phosphate supersaturated environment of saliva (*1*−*7*). Statherin also serves as an important boundary lubricant (*8*, *9*) and as a mediator of bacterial adhesion in periodontopathologies (*10*, *11*). Recent studies have correlated cancerous lesion diagnosis in the oral cavity with deficiencies of statherin in salivary glands (*12*). The molecular mechanisms underlying the interaction of statherin with HAP have been extensively studied to deduce how proteins recognize and function at the organic−inorganic biomineral interface.

The primary structure of statherin (Table 1) exhibits charge asymmetry with most of its ionizable amino acids located in its amino-terminal region (residues 1−13) (*1*). The sequence of the first five negatively charged amino acids, DpSpSEE (where pS denotes a phosphorylated serine), is directly involved in hydroxyapatite binding (*5*, *13*). The presence of acidic amino acid segments is a common motif in proteins controlling biomineralization processes. It is followed by a segment that is rich in positively charged residues with one lysine at position 6 and three arginines at positions 9, 10, and 13. The only additional charged amino acid is glutamic acid at position 26.

Structural and dynamic studies of statherin and statherin fragments adsorbed onto hydroxyapatite have been carried out by our group using high-resolution solid-state nuclear magnetic resonance (ss-NMR) (*14*−*20*). The results demonstrated that the N-terminal domain of the protein (residues 1−12) adopts an α-helical structure upon adsorption and that the acidic residues are in close proximity to the HAP surface. The helix is amphipathic with the side chains of the charged amino acids pointing in a direction opposite to that of the neutral amino acids. Figure 1a illustrates the orientation of consecutive side chains along the helical axis of the N-terminus of statherin. The importance of the α-helical motif in the recognition of HAP by statherin is analogous to the role of a similar motif in the binding of osteocalcin to HAP (*21*). Relaxation measurements of carbonyl atoms along the backbone illustrated that the acidic statherin N-terminus is immobilized on the HAP surface, whereas the rest of the N-terminal domain is more mobile and, therefore, might

† This work was supported by funding from the National Institutes of Health (grant DE12554) and the National Science Foundation (grants 0502177 and 9807748).

* Corresponding author. Phone: 206-685-8148. Fax: 206-616-3928. E-mail: stayton@u.washington.edu.

‡ Department of Bioengineering, University of Washington.

§ Department of Chemistry, University of Washington.

|| Pacific Northwest National Laboratory.

[1] Abbreviations: CP, cross-polarization; CSA, chemical shift anisotropy; HAP, hydroxyapatite $Ca_{10}(OH)_2(PO_4)_6$; HB, Herzfeld−Berger; ITC, isothermal titration calorimetry; PB, phosphate buffer composed of the following compounds: 100 mM NaCl, 40 mM KCl, 4.3 mM Na_2HPO_4, and 1.4 mM KH_2PO_4 at pH 7.4; PI, isoelectric point; REDOR, rotational echo double resonance; RT, room temperature; ss-NMR, solid-state nuclear magnetic resonance.

10.1021/bi602345a CCC: $37.00
Published on Web 03/29/2007

Table 1: Amino Acid Sequence of Native Statherin and the Mutants Studied[a]

stath(WT)	DpSpSEE*K*FL***RR*IG**R*FGYGYGPYQPVPEQPLYPQPYQPQYQQYTF
stath(K6A)	DpSpSEE**A**FL*RRIG*RFGYGYGPYQPVPEQPLYPQPYQPQYQQYTF
stath(R9A)	DpSpSEEKFL****A**RIG*RFGYGYGPYQPVPEQPLYPQPYQPQYQQYTF
stath(R10A)	DpSpSEEKFL*RA**A**IG*RFGYGYGPYQPVPEQPLYPQPYQPQYQQYTF
stath(R13A)	DpSpSEEKFL*RRIG****A**FGYGYGPYQPVPEQPLYPQPYQPQYQQYTF
stath(KRA)	DpSpSEE**A**FL****AA**IG****A**FGYGYGPYQPVPEQPLYPQPYQPQYQQYTF

[a]All proteins were labeled at positions L_8 ($^{13}C{=}O$) and G_{12} (^{15}N) for ss-NMR structure and dynamics measurements (indicated by *). The residue positions mutated to alanine are indicated in italics in the wild-type sequence and highlighted in bold in the mutated sequences.

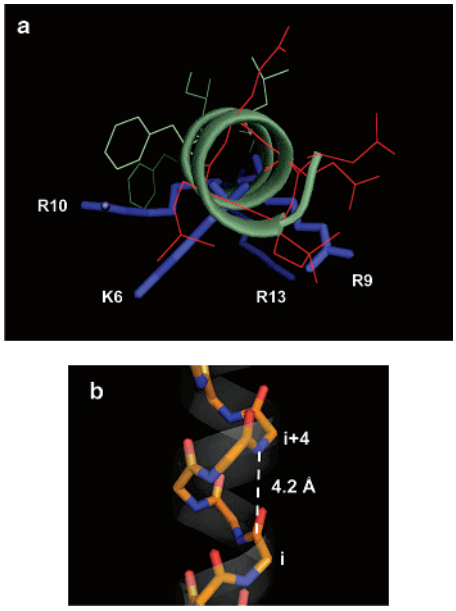

FIGURE 1: (a) Representation of the side-chain orientation of stath-(WT) along the helical axis of the protein's N-terminus illustrating its amphipathic nature. The amino acid side chains are colored as follows: basic, blue; acidic, red; and neutral, green. (b) α-Helical representation showing the structural measurement made across the *i* and *i* + 4 residues.

interact more weakly with the HAP surface (*17*). Recently, ss-NMR measurements have shown that statherin adopts a compact folded conformation upon binding to HAP with a second α-helical motif at the C-terminus of the protein that interacts with the proline-rich domain in the protein (*20*).

In a recent study, we proposed a more detailed adsorption model that connected thermodynamic binding parameters to the electrostatic interactions between the charged amino acids and the mineral surface (*22*). These measurements and the model were in accordance with the direct role of the acidic motif at the N-terminus of statherin binding to HAP (*5*, *13*, *17*). Here, we have probed the role of the corresponding basic segment in hydroxyapatite recognition by studying single point and multiple mutations. These positively charged residues were systematically replaced with alanine, and the binding of the mutants to HAP was studied using equilibrium adsorption isotherm analysis and isothermal titration calorimetry (ITC). The structure of the adsorbed proteins was characterized using ss-NMR rotational echo double resonance (REDOR) (*23*, *24*), and dynamics were characterized using cross-polarization magic angle spinning measurements with Herzfeld−Berger analysis of the sideband manifolds (*25*) and rotating-frame relaxation ($T_{1\rho}$) measurements (*26*). It was found that single point mutations lowered the binding affinity to HAP but did not significantly alter the packing density of statherin at binding saturation, whereas the simultaneous mutation of all four basic amino acids substantially reduced the binding affinity and the maximum surface coverage without modifying the secondary structure and dynamic properties of the N-terminal domain.

MATERIALS AND METHODS

Hydroxyapatite Preparation. Hydroxyapatite seed crystals with a density of 0.032 g/mL were generously provided by Allison Campbell, Battelle Pacific Northwest National Laboratory (*27*). X-ray powder diffraction (Phillips) confirmed the formation of HAP and the absence of other unwanted calcium phosphate phases. BET (Quantachrom) measurements showed a specific surface area of 53 m^2/g. The calcium (Ca) to phosphorus (P) ratio, measured by inductively coupled ion plasma (ICP) spectroscopy, was determined to be 1.67. Crystal morphology as determined by electron microscopy (using scanning and transmission modes) was as expected for hydroxyapatite.

Protein Synthesis. Statherin and its mutants were synthesized using standard Fmoc solid-phase synthesis as previously described (*22*). L-Leucine-*N*-Fmoc (1-^{13}C,99%) and glycine-*N*-Fmoc (^{15}N,98%) were purchased from Cambridge Isotope Laboratories and incorporated into the solid-phase peptide synthesis without further treatment.

Protein Purification and Characterization. Protein purification was performed as previously described using a 10mmD/100mmL, 7.9 mL POROS HQ/M strong anion exchange column plumbed to a BioCAD SPRINT Perfusion Chromatography System (*22*). Briefly, the mobile buffer consisted of A with 50 mM Tris-HCl at pH 8.5, B with buffer A + 0.5 M NaCl, and C with 30% acetonitrile. A linear gradient of 0% to 70% B in 14.7 column volumes was used to elute the protein. Stath(WT), stath(R9A), stath(R10A), and stath(R13A) eluted at 35% buffer B. Stath(K6A) and stath-(KRA) eluted at 43 and 53% buffer B, respectively. The pure proteins (>90%) were characterized by electrospray ionization mass spectrometry, and their concentrations were determined from amino acid analysis. The calculated isoelectric points (PI) of stath(WT) and stath(KRA) are 4.41 and 2.07, respectively. The calculated PIs of the single mutated proteins are 4.01 (*28*).

Equilibrium Adsorption Binding Isotherm. In adsorption experiments, known amounts of statherin and its mutants (5−70 μM) were equilibrated for 4 h with HAP suspension (0.5 mg/0.5 mL) at 25 °C in phosphate buffer (PB) with the following composition: 100 mM NaCl, 40 mM KCl, 4.3 mM Na_2HPO_4, and 1.4 mM KH_2PO_4, pH 7.4. Samples were prepared in triplicate for each protein concentration. After incubation, the protein concentrations in the supernatant were determined using a Micro BCA protein assay reagent kit (Pierce). The amount of protein on the HAP surface was determined by subtracting the measured quantity from the

initially added amount. Matlab function FMINS, which minimizes a function of several variables using the Nelder−Mead simplex method, was used to calculate the χ^2 function to fit the experimental data (*29*).

Isothermal Titration Calorimetry. ITC experiments were carried out on a VP-ITC system (Microcal, LLC.) at 25 °C. All experiments were performed in PB with both the protein and mineral initially in the same buffer. For all experiments, protein (0.14−0.16 mM) was injected in 25 μL increments into the isothermal calorimeter cell (1.42 mL) pre-filled with a HAP suspension in buffer. To determine the enthalpy at the initial steps of adsorption, 6 mg/mL of HAP was titrated with 4 injections of 25 μL protein solution, and the amount of free and adsorbed protein was determined. Full titration experiments were performed with stath(WT) and stath(KRA) and with HAP suspensions of 2 and 4 mg/mL, respectively. HAP was titrated using 17 to 22 injections of 25 μL protein solution. To minimize the error associated with diffusion from the syringe during baseline equilibration, the first injection was only 5 μL, and the associated small heat signal was not included in data analysis. A 4-min interval was allowed between injections for equilibration of the adsorbed protein; this period was sufficient for the complete return of the heat signal to baseline. A blank experiment where the protein was injected into a HAP suspension's supernatant (no HAP) was carried out and was used to correct the data due to dilution.

Solid-State NMR. All NMR experiments were performed on a Chemagnetics Infinity console at 300 MHz proton frequency with a Chemagnetics triply resonant variable temperature probe. Chemical shifts were referenced to glycine $^{13}C{=}O$ (177 ppm) (*30*). Rotational echo double resonance (REDOR) (*23*, *24*) data were collected at −35 °C at a spinning speed of 4000 Hz and a 1 s recycle time, using the XY8 pulse sequence with a typical set-up utilizing a 14.3 μs π-pulse for carbon (observe) and a 12.9 μs π-pulse for nitrogen (dephasing). The cross-polarization (CP) condition utilized a 6 μs 90° ^{1}H pulse and a 0.8 ms mixing time, with a two-pulse-phase-modulated (TPPM) decoupling field of ∼65 kHz used throughout. Thirteen data points were collected out to 104 rotor cycles, averaging 1024−10240 scans and repeating 5−7 times. A typical protein-HAP sample was approximately 50−90 mg. REDOR dephasing curves were simulated using a C^{++} code operating in a Matlab environment, which incorporated the chemical shift anisotropy of the carbonyl carbon spin and experimental parameters of the applied radiofrequency pulses.

$T_{1\rho}$ and Herzfeld−Berger (HB) analyses were used to extract protein dynamics (*25*, *26*). Both experiments utilized a 42 kHz CP field with a contact time of 0.5−1 ms and a pulse delay of 3 s and were measured at both room temperature and −35 °C. The HB experiment utilized a 1500 Hz spinning speed and collected 28800 scans at each temperature. The asymmetry ($\eta = |(\sigma_{22}-\sigma_{11})|/(\sigma_{33}-\sigma_{iso})$) and the anisotropy ($\Omega = (\sigma_{33}-\sigma_{11})$) were determined by modeling the observed center and side band peak intensities. The $T_{1\rho}$ data were taken at 10 spin−lock intervals ranging from 0.05 to 4.55 ms and at a spinning speed of 4000 Hz. Typically 1024 scans were collected at −35 °C and 4096 scans at room temperature. Errors in the reported NMR parameters were computed from experimental signal-to-noise ratios and from standard deviations of the values in repeated experiments.

Protein/HAP Surface Binding for NMR Measurements. A typical surface binding protocol for the NMR measurements follows. Protein synthesis yielded different amounts of pure protein for the different mutants. To standardize the adsorption to HAP, the weighed proteins were dissolved in PB to achieve a protein concentration of 3.6×10^{-5} (±0.1) M for all mutants. The hydroxyapatite suspension (1 mg/mL) volume used for adsorption of the different mutants was adjusted as well to maintain a w/w ratio of 3 to 10 between the protein and the mineral. An aliquot of the HAP suspension was centrifuged, washed 3 times with 5 mL PB, and subsequently added to the protein solution. After binding while stirring for 4 h at room temperature, the sample was quickly spun down, washed 3 times with 10 mL PB to remove any nonspecifically bound protein, and left hydrated with the consistency of a thick paste.

RESULTS

The amino acid sequences of native statherin and the various mutants studied here are given in Table 1 (see Figure 1a for residue locations in the structure). The specific positions on the protein backbone isotopically labeled for the NMR measurements are also indicated in Table 1.

Equilibrium Adsorption Isotherm Measurements. The equilibrium isotherms for the adsorption of native statherin and the various mutants (Table 1) onto HAP at 25 °C are shown in Figure 2 as the number of moles adsorbed per unit of surface area, N, versus the equilibrium concentration of free protein in solution [C]. The measured data points were collected sequentially with increasing [C], allowing 4 h for equilibration at each concentration.

As was previously observed for statherin (*4*, *5*, *22*), the adsorption data of the native protein and the mutants exhibit a reasonably good fit to a simple first-order Langmuir adsorption isotherm according to the following equations:

$$N = \frac{KN_{max}[C]}{1 + K[C]} \tag{1a}$$

$$\theta = \frac{K[C]}{1 + K[C]} \tag{1b}$$

and

$$K = \frac{\theta}{(1 - \theta)[C]} \tag{1c}$$

where N_{max} is the maximum number of binding sites per unit surface area, K is the equilibrium binding constant, and $\theta = N/N_{max}$ is the fractional coverage. The best-fit values for K and N_{max} are reported in Table 2, with observed values for stath(WT) that are similar to those previously reported (*22*). The standard Gibbs free energy change (ΔG^0) calculated from the equation $\Delta G^0 = -RT \ln K$ is also reported in Table 2, together with the $\Delta\Delta G^0$ values calculated relative to that of wild-type statherin. From Table 2, it is notable that the equilibrium binding constants for the single point mutants are 1.5−2.5-fold lower than that for stath(WT) and that there is no significant difference in the N_{max} values. For the multiply mutated protein stath(KRA), there is a 5-fold

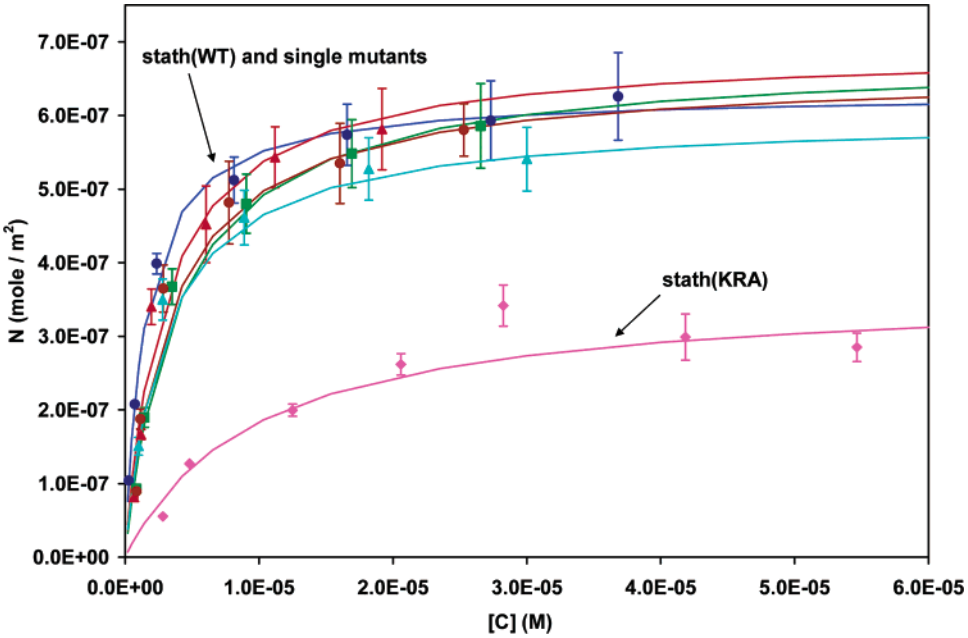

FIGURE 2: Adsorption isotherms of native statherin (blue ●), stath(K6A) (red ▲), stath(R9A) (green ■), stath(R10A) (aqua ▲), stath(R13A) (brown ●), and stath(KRA) (magenta ◆) on HAP at 25 °C. The data points represent the average of three independent measurements. The solid lines represent the best fit to a first-order Langmuir model (eqs 1a−c).

Table 2: Thermodynamic Parameters for Adsorption of Statherin and Its Mutants onto HAP at 25 °C[a]

protein	N_{max} (10^{-7}mol/m^2)	K (10^5/M)	ΔG^0 (kcal/mol)	$\Delta\Delta G^0$ (kcal/mol)	$\Delta H_{initial}$[b] (kcal/mol adsorbed)
stath(WT)	6.2 ± 0.7	7.0 ± 0.9	−7.9 ± 0.1		−3.3 ± 0.4, 90%
stath(K6A)	7.3 ± 0.9	2.8 ± 0.6	−7.4 ± 0.1	0.5 ± 0.1	−3.7 ± 0.5, 85%
stath(R9A)	6.8 ± 0.3	2.8 ± 0.5	−7.4 ± 0.1	0.5 ± 0.1	−3.2 ± 0.3, 85%
stath(R10A)	5.7 ± 0.8	4.5 ± 1.2	−7.6 ± 0.2	0.3 ± 0.2	−3.8 ± 0.4, 85%
stath(R13A)	6.4 ± 0.8	4.0 ± 1.0	−7.6 ± 0.2	0.3 ± 0.2	−3.1 ± 0.3, 85%
stath(KRA)	3.0 ± 1.2	1.5 ± 0.8	−7.0 ± 0.3	0.9 ± 0.3	−3.7 ± 0.4, 45%

[a] N_{max}, K, ΔG^0, and $\Delta\Delta G^0$ were obtained from equilibrium adsorption binding isotherms. $\Delta\Delta G^0$ is given relative to stath(WT). $\Delta H_{initial}$ was obtained from ITC and is defined as the initial enthalpy of adsorption onto site A given per mole of protein adsorbed. The errors reported are based on two standard deviations in the χ^2 (N_{max} ,K) analysis of the binding isotherms data. Construction of the χ^2 function took experimental error into account. [b] The percentage of the total injected protein that adsorbs in the first calorimetric injection is given (with the rest remaining in solution in the cell of the calorimeter).

decrease in the K value relative to that of the wild type, which is reflected by the requirement for much higher free stath-(KRA) concentrations to achieve the same coverage relative to saturation (see Figure 2). Moreover, stath(KRA) adsorption is saturated at an N_{max} value that is about twice as low as the maximal coverage observed for stath(WT).

In a recent article (*22*), we have proposed that the adsorption process of statherin onto HAP occurs through at least two distinct processes. The initial process **A** is described by a simple Langmuir model that is associated with a measurable molar enthalpy of adsorption (as observed from calorimetric measurements). The subsequent process **B** does not exhibit a measurable heat of adsorption and is more adequately described by a coverage-dependent binding model with favorable protein−protein interactions. The adsorption isotherm measurements reported here had to employ smaller HAP samples with the mutant statherins, with a surface area of only 0.026 m^2, 2 to 5 times lower than that in the previous work. Consequently, the sensitivity of the determination of the free and bound mutant protein concentration is markedly lowered, as seen in the error bars calculated for each point in the isotherms in Figure 2. For this reason, the adsorption thermodynamic comparisons between the mutants and the native protein are insensitive to differential changes in adsorption with increasing coverage, and the data sets have all been fit with a simple first-order Langmuir model.

Isothermal Titration Calorimentry. In order to study the effects of the basic amino acids on the enthalpy related to the initial adsorption onto site A, we have used ITC to detect the heat exchanged during the titration of HAP with stath-(WT) and stath(KRA) (Figure 3). Note that because N_{max} for stath(WT) is ca. 2-fold higher than that of stath(KRA) (Table 2), a larger amount of mineral is used for the mutant (Figure 3) in order to maintain the same total molar concentration of adsorption sites (M_t') on the mineral surface per unit volume in the ITC cell (*22*):

$$M_t' = N_{max}\frac{\text{moles}}{m^2} \times SA\frac{m^2}{g} \times D\frac{g}{L} \qquad (2)$$

where SA is the specific surface area of the HAP (per gram) obtained from BET measurements, and D is the amount of HAP placed in the ITC cell (in grams) per unit volume of the ITC cell. Figure 3a displays the detected heat per mole of injected protein as a function of C_t/M_t', where C_t is the total concentration of the protein in the ITC cell. It is seen in Figure 3a that the initial adsorption of both stath(WT) and stath(KRA) onto HAP is driven by an exothermic

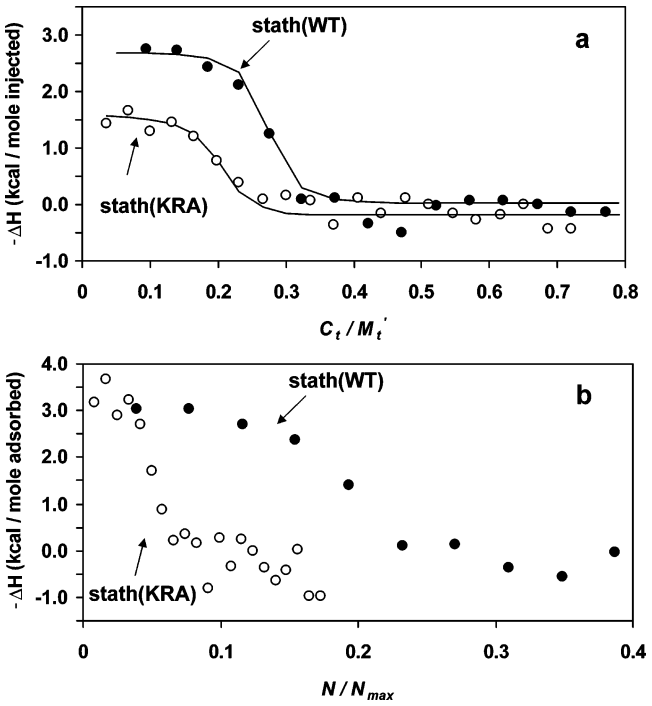

FIGURE 3: ITC titration curves of HAP (2 mg/mL) with stath(WT) (0.16 mM) (●) and HAP (4 mg/mL) with stath(KRA) (0.14 mM) (○) performed at 25 °C in PB. The curves were corrected for heat of dilution and plotted as (a) heat released per mole of injected protein as a function of the molar ratio between the total injected protein concentration, C_t, and the molar concentration of adsorption sites on HAP, M_t'. (Note that M_t', calculated from eq 2, is similar for both proteins.) The data points above $C_t/M_t' = 0.4$ illustrate the scattering of the data that together with the relatively low heat signal result in ~15% uncertainty in the detected heat of adsorption for stath(KRA). The data points were fit (solid line) as described previously (*22*). (b) Heat released per mole of adsorbed protein vs coverage. Note that N_{max} of stath(WT) was used in (b) for both proteins.

Table 3: Apparent Thermodynamic Parameters for the Adsorption of stath(WT) and stath(KRA) onto HAP A Sites Obtained from ITC at 25 °C

protein	ΔH_{app} (kcal/mol)	$T\Delta S$ (kcal/mol)	ΔG^0 (kcal/mol)	K_A (1/M)
stath(WT)	-3.0 ± 0.4	6.1 ± 0.4	-9.2 ± 0.6	$(5.4 \pm 5.7) \times 10^6$
stath(KRA)	-1.7 ± 0.3	7.3 ± 0.6	-9.0 ± 0.6	$(4.8 \pm 4.0) \times 10^6$

enthalpy. However, the detected heat upon the titration of HAP with stath(KRA) is about half that of the native protein. For both proteins, the heat signal drops to close to zero at a C_t/M_t' ratio of 0.3. Repeated experiments with half the amount of HAP in the ITC cell (2 mg/mL) for stath(KRA) gave similar titration curves.

The basic model used to derive the expression for a typical ITC titration curve is identical to a first-order Langmuir adsorption model (eq 1c), as previously shown (*22*). The equilibrium binding constant for A sites and the apparent adsorption enthalpy were determined from the ITC titration curves (Figure 3a). These thermodynamic parameters, together with the Gibbs free energy and binding entropy, are reported in Table 3. The values for stath(WT) are consistent with previously reported values (*22*). The equilibrium binding constant to HAP A-sites for the stath(KRA) protein is of the same order of magnitude as that for the wild type but with a relatively large uncertainty in the recovered value resulting from a low signal-to-noise ratio in the ITC experiment. Therefore, it is difficult to determine whether differences in binding constants to A sites exist for stath(KRA) relative to native statherin. For both proteins, however, the K values for the A-sites are higher than the overall equilibrium constant determined independently from the adsorption isotherm (Table 2). We had previously shown that the binding isotherm predominantly measures the binding to the thermoneutral B sites, which constitute the majority of binding sites on HAP (*22*). We, therefore, conclude that the overall equilibrium constant for stath(KRA) is 5-fold lower relative to that for the native protein as was calculated from the adsorption binding isotherm (Figure 2 and Table 2).

The calorimetric results were combined with the equilibrium adsorption isotherm data to calculate the enthalpy per mole of adsorbed protein versus the fractional coverage of surface sites, N/N_{max} (normalized to N_{max} of stath(WT) for both proteins), as shown in Figure 3b. Interestingly, both proteins adsorb to the mineral with a similar enthalpy per mole of adsorbed protein in the initial adsorption steps, $\Delta H_{initial}$ (first injections) (Table 2). However, the heat of adsorption drops close to zero at ~30% of binding saturation (maximal molecules per unit area) for the native protein, whereas the heat signal for stath(KRA) saturates at only ~7.5% of the total sites for stath(WT). Thus, the saturation coverage of this mutant on A sites (i.e., the sites for initial adsorption that have a measurable heat of adsorption) is only about one-quarter of that for stath(WT). Nevertheless, the initial heat of adsorption (approximately −3 kcal/mol) is about the same (Table 2), implying that the contribution of the basic amino acids to the enthalpy of adsorption via specific interactions with the mineral is not significant.

Statherin mutants with only one of the basic acids mutated to alanine show an overall adsorption behavior that is very similar to that of the native protein (Figure 2 and Table 2). We performed ITC measurements with these mutants to determine the initial enthalpy of adsorption onto the proposed A sites. An excess of HAP crystals (6 mg/mL) in the ITC cell were titrated with four repeated injections (25 μL) of each protein (0.14−0.16 mM) at 25 °C. The amount of HAP used was sufficient to ensure the detection of a constant heat signal before reaching saturation, and the experiment was performed up to a $N/N_{max} = 0.05$ value. The apparent heat detected for all of these mutants was very similar to that detected for stath(WT), resulting in a very similar initial enthalpy per mole adsorbed protein (Table 2).

These results indicate that the individual basic amino acids contribute very little to the enthalpy of statherin adsorption onto HAP A sites. Although the simultaneous mutation of the basic amino acids does not affect the adsorption enthalpy of individual statherin molecules onto HAP (i.e., enthalpy per mole protein), it lowers the total heat associated with the adsorption process only because fewer stath(KRA) molecules compared to the number of wild type or single mutants adsorb onto the mineral in total (Figure 3b).

Structure. A strong secondary structural determinant in proteins is the $i \rightarrow i + 4$ backbone carbonyl carbon to backbone amide nitrogen distance. In the helical structure, this distance is as short as 4.2 Å (illustrated in Figure 1b) because of the hydrogen bond formed between the carbonyl oxygen and the amide proton, whereas in the β-sheet

Table 4: Summary of $^{13}C-^{15}N$ Distance Measurements (−35 °C), ^{13}C Chemical Shift, and Line Width Data (RT and −35 °C) for Statherin and Its Mutants Bound to HAP (Hydrated)

protein	C−N distance (Å)	chemical shift (ppm) −35 °C	chemical shift (ppm) RT	line width (ppm) −35 °C	line width (ppm) RT
stath(WT)	4.6 (±0.5)	175.2 (±0.5)	176.9 (±0.5)	7.4	7.3
stath(K6A)	4.2 (±0.5)	176.2 (±0.5)	178.3 (±0.5)	6.1	4.1
stath(R9A)	4.5 (±0.5)	176.6 (±0.5)	176.8 (±0.5)	7.6	3.6
stath(R10A)	4.6 (±0.5)	175.4 (±0.5)	176.8 (±0.5)	7.6	5.3
stath(R13A)	4.4 (±0.5)	176.1 (±0.5)	177.1 (±0.5)	7.6	5.3
stath(KRA)	4.3 (±0.5)	176.3 (±0.5)	176.9 (±0.5)	7.9	7.2

Table 5: Summary of Dynamics Data: Rotating-Frame Relaxation ($T_{1\rho}$) and CSA (η/Ω) for Statherin and Its Mutants at RT and −35 °C

protein	$T_{1\rho}$ (ms) −35 °C	$T_{1\rho}$ (ms) RT	η/Ω (ppm) −35 °C	η/Ω (ppm) RT
stath(WT)	26.2 (±1.6)	11.4 (±1.7)	0.7 (±0.1)/137 (±20)	0.7 (±0.1)/131 (±20)
stath(K6A)	18.2 (±1.1)	10.7 (±1.6)	0.6 (±0.1)/147 (±20)	0.5 (±0.1)/138 (±20)
stath(R9A)	26.9 (±1.6)	8.0 (±1.2)	0.6 (±0.1)/143 (±20)	0.6 (±0.1)/98 (±20)
stath(R10A)	31.7 (±2.0)	8.5 (±1.3)	0.7 (±0.1)/143 (±20)	0.6 (±0.1)/134 (±20)
stath(R13A)	16.4 (±1.0)	10.3 (±1.5)	0.7 (±0.1)/145 (±20)	0.7 (±0.1)/122 (±20)
stath(KRA)	36.2 (±2.2)	11.4 (±1.7)	0.7 (±0.1)/159 (±20)	0.5 (±0.1)/143 (±20)

structure, it is greater than 10.0 Å, making it an ideal probe for local structural measurements. Structural studies in the N-terminal domain of the statherin mutants probed the distance and, consequently, the secondary structure from $L_8 \rightarrow G_{12}$, backbone ^{13}C carbonyl labeled to backbone ^{15}N amide, respectively (Table 1). Previous studies have shown this region to be helical for the surface-immobilized statherin (*17*) and thus a good indicator of a change in structure for mutants encompassed within or close to this region.

The $(^{13}C)L_8-(^{15}N)G_{12}$ distances measured from the CN-REDOR dephasing curves (Figure 1 in Supporting Information) for the adsorbed statherin mutants are summarized in Table 4. These distances in statherin and in all of its mutants range between 4.2 and 4.6 Å. Within the error in these measurements (±0.5) Å, all mutants exhibit similar short $(^{13}C)L_8-(^{15}N)G_{12}$ distances, indicating that the helical backbone fold in the vicinity of the mutation sites is preserved.

Chemical shift values can also be qualitative indicators of structural changes, though absolute values are difficult to interpret on a charged surface such as hydroxyapatite. The L_8 $^{13}C{=}O$ chemical shift of each of the adsorbed proteins was measured both when frozen and at RT. The spectra are referenced to glycine (177.0 ppm), and the results are summarized in Table 4. The measured chemical shift is very similar for the protein−HAP complexes both when frozen and at RT, with the average shifting slightly downfield at room temperature from 176.4 to 177.1 ppm. The line widths of the carbonyl carbon resonance in the different proteins are 6.1−7.9 ppm at −35 °C (Table 4), possibly indicating structural dispersion, but other inhomogeneous broadening could also be a contributing factor, as has been suggested previously (*16*). For all of the mutants, the line narrows to 3.6−7.3 ppm at RT (Table 4), possibly due to the increase in dynamics with temperature. Within the certainty in the line width determination, no substantial change that might indicate change in secondary structure is detected in the chemical shift of the L_8 $^{13}C{=}O$ carbonyl line in the mutants relative to the native protein. On the basis of the distance measurements and the chemical shift information, we conclude that there is no major change in structure for the mutants compared to that of the native protein.

Dynamics. The dynamics of statherin and mutants were measured on the ^{13}C carbonyl of L_8 in the backbone of the protein using $T_{1\rho}$ and Herzfeld−Berger (HB) analysis of the side band manifold (*25*, *26*). All dynamics were measured both when frozen and at RT, hydrated under both conditions (Table 5 and Figure 2 in Supporting Information). The frozen stath(WT) showed a typical side band pattern for an immobile carbonyl chemical shift anisotropy (CSA), with an η of 0.7 and an anisotropy of 137 ppm. The $T_{1\rho}$ for the frozen protein−HAP complex was also typical of an immobile carbonyl, with a decay of 26.2 ms. At room temperature, neither η nor Ω changed significantly, with values of 0.7 and 131, respectively. However, the signal intensity dropped substantially by a factor of ∼10 for the RT sample compared to that for the frozen sample (Figure 4), and $T_{1\rho}$ decreased to 11.4 ms for the RT sample, indicating an increase in mobility. The observations are consistent with an interpretation that the frequency, but not the amplitude of protein motion is increasing when the protein/HAP complex is not frozen (*17*).

For the frozen protein−HAP complex, the $T_{1\rho}$ values in the mutants and the wild-type protein are, as expected, very similar. The asymmetry and anisotropy are also essentially unchanged within the error of the measurement. For the protein−HAP complex at RT, the $T_{1\rho}$ values of the mutants vary from 8.0 to 11.4 ms, well within the range of error but significantly faster than the frozen complex (Table 5). The line shape in all cases has not substantially changed. The anisotropy has consistently shifted closer to 0.6 (ranging from 0.5 to 0.7), whereas the average anisotropy of the CSA has narrowed slightly to 127 ppm compared to 145 ppm for the frozen sample. Although some of the η and Ω values for individual mutants are lower, these are determined to be within the signal-to-noise ratios of the spectra.

DISCUSSION

Perhaps the most notable property of statherin from a primary amino acid sequence perspective is the presence of an N-terminal acidic sequence followed by a segment with four basic amino acids. Although the initial acidic amino acid segment has been studied in some detail, the basic segment is largely uncharacterized. The existence of statherin isoforms lacking the basic residues found in the 6−15 region has been previously reported (*31*). These isoforms constitute

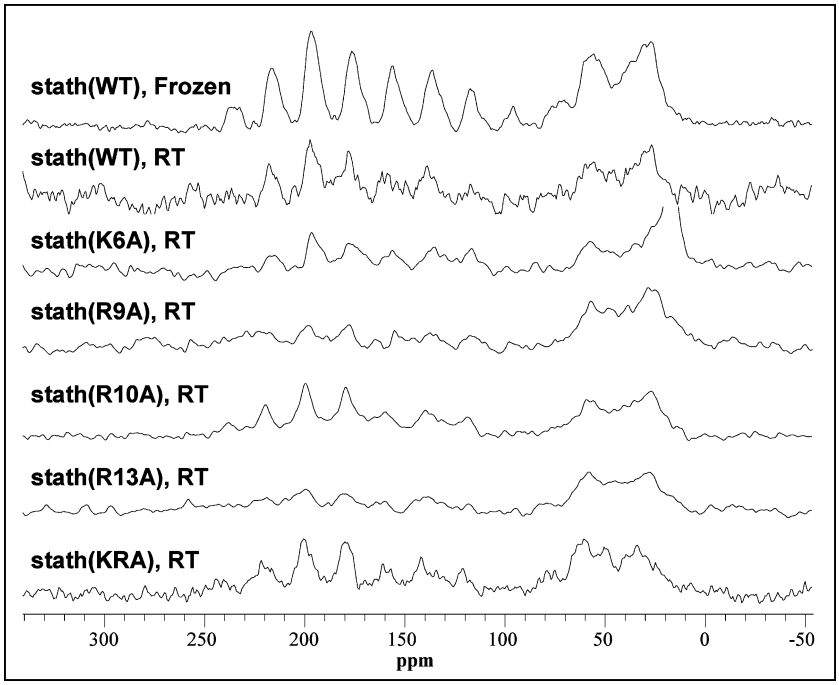

FIGURE 4: ^{13}C NMR spectra of statherin and mutants. The frozen wild type is shown at the top for the comparison of an immobile CSA. Following from top to bottom are stath(WT), stath(K6A), stath(R9A), stath(R10A), stath(R13A), and stath(KRA) under hydrated conditions. All of the mutants show a significant decrease in signal intensity as a function of hydration, indicating mobility. However, there is little evidence of a decrease in CSA, bracketing the motion to 10^{-3} to 10^{-5} s.

a small fraction of statherin concentration in saliva and are believed to be the result of post-translational modifications and alternative splicing of the statherin gene (*32*). Although there have been no functional studies of these statherin isoforms, these findings provide an additional biological rationale for studying the role of the basic amino acids.

The single basic amino acid mutants of statherin displayed a conserved α-helical structure in the N-terminus, similar to the native protein on hydroxyapatite, and conserved carbonyl backbone dynamic features at position L_8. They exhibit a small decrease in binding affinity to HAP crystals, but the single mutations do not alter the maximal binding coverage at saturation. The stath(KRA) mutant with all basic side chains mutated to alanine displayed conserved structural and dynamic properties on hydroxyapatite, but had a substantially reduced binding affinity (5-fold reduction) and lowered maximal surface coverage (∼1/2) (Figure 2 and Table 2).

All of the proteins in Table 1 are negatively charged at pH 7.4, with a calculated PI of 4.41 and 2.07 for stath(WT) and stath(KRA), respectively, and a PI of 4.01 for all of the single mutants (*28*). Because of its relatively higher negatively charged N-terminus, stath(KRA) should have an ∼3-fold higher net negative charge at this pH than that of stath(WT) and twice the negative charge of the single mutants. The higher negative charge of stath(KRA) could give rise to repulsive electrostatic interactions between protein molecules that adsorb to the mineral surface. These repulsive interactions would hinder the close packing of stath(KRA) molecules on the surface, yielding the lower saturation coverage observed for this mutant.

An analysis of the adsorption thermodynamics of native statherin previously led us to propose a mechanism that involves two types of binding sites on the HAP surface. The A site populates first with constant exothermic heat of adsorption (approximately −3 kcal/mol), and the B site displays zero heat of adsorption and is populated primarily after the A sites are saturated. The mechanism of the entropic adsorption to B sites was suggested to involve bound-water release and favorable protein−protein interactions at higher coverage (*22*), consistent with the tendency of statherin to form dimers in solution (*33*, *34*).

We show here that all mutants exhibit two-site adsorption similar to that of the native protein. Furthermore, we show that the initial enthalpy of adsorption to A sites for all of the mutants is very similar to that of stath(WT) (Table 2), implying that any contribution of the basic amino acids to the enthalpy of adsorption via interactions with the mineral is small enough to be undetectable by our isothermal titration calorimeter. The ITC data in conjunction with the coverages determined from the overall adsorption isotherm measurements (Figure 3b) reveal that only ∼25% as many stath(KRA) molecules adsorb to the A sites with this enthalpy (approximately −3 kcal/mol) compared to amount of stath(WT) or single mutants. Repulsive interactions that increase the excluded area for protein−protein interactions will only be effective in reducing the maximal coverage if the A sites are clustered on the surface of hydroxyapatite. The A sites could correspond, for example, to step edges or high-energy crystal faces of the mineral surface.

The lower equilibrium constant of stath(KRA) adsorption to HAP relative to that of the native protein constitutes a less favorable Gibbs free energy for this mutant with a $\Delta\Delta G^0$ value that is ∼11% of the total ΔG^0 of native statherin adsorption (see Table 2). Because the binding enthalpy is comparable between the native protein and the stath(KRA) mutant for adsorption to both the A and the B sites, a less positive binding entropy for stath(KRA) can be inferred. Changes to the individual factors that contribute to the overall adsorption entropy can explain the less favorable entropy. Stath(KRA) adsorption may be accompanied by the release

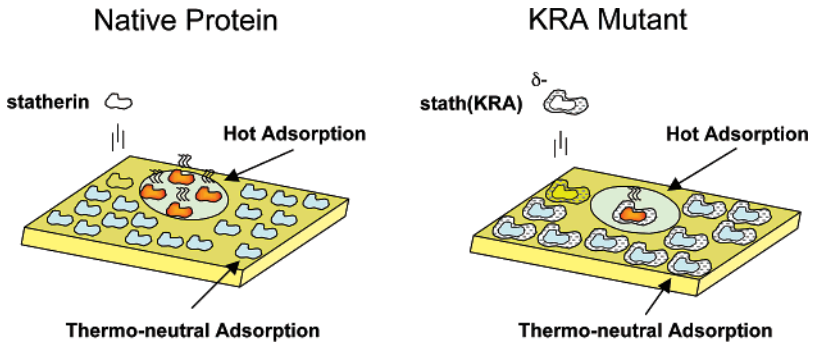

FIGURE 5: Illustration of the adsorption onto HAP of the native protein (left) and the stath(KRA) mutant (right) in which all positively charged amino acid residues were replaced by alanine residues. Stath(KRA) molecules are drawn with an additional gray area surrounding them with δ- representing the larger effective footprint on the surface and the higher charge at the pH used in the experiments. Orange colored protein molecules are associated with exothermic adsorption to A sites on HAP. Light-blue colored protein molecules are associated with thermo-neutral adsorption to B sites on HAP. Adsorption through the two processes for the two species is shown with the relative ratio of molecules adsorbed as derived from the measurements.

of fewer water molecules due to less favorable protein−surface or protein−protein interactions. The adsorbed mutant molecules may experience restricted motions relative to the native protein molecules that are not captured in the limited NMR dynamic studies reported here. It may also be a net effect of the aforementioned terms and others that manifest themselves in smaller entropy. Because we do not observe any change in heat as B sites are occupied, we conclude either that the enthalpic contribution from protein−protein interactions is cancelled by other processes or that it is lower than the detection level in the ITC calorimeter.

The results reported here are summarized in a descriptive model for the adsorption of native statherin and the stath-(KRA) mutant shown in Figure 5. The higher negative charge on the mutant is denoted by a δ- close to it and by the shaded area surrounding the protein molecule. This illustrates that the stath(KRA) mutant could induce a larger excluded volume due to electrostatic repulsions between proteins at physiological pH. The exothermic adsorption of protein molecules to A sites is illustrated in Figure 5 by orange colored protein molecules attached to light green bound ellipsoids. The experimentally determined ratio of 4:1 between statherin and stath(KRA) molecules occupying the A sites as well as the ratio of 2:1 between the native protein and the mutant occupying B sites at saturation of these processes is also illustrated in Figure 5. The similarity in the enthalpy for the two species is implied by using the same colors for statherin and stath(KRA) molecules. The clustered proteins on the mineral surface underscore differences in protein−protein interactions between the two species in the early adsorption process (A sites) as well as during the adsorption to B sites.

CONCLUSIONS

The different functions of native statherin at the tooth enamel surface rely on an efficient binding to hydroxyapatite surfaces. We have shown here that taken individually, none of the individual basic amino acids of statherin are crucial for the binding of the protein to HAP crystals. However, as a group they substantially decrease the overall charge of the protein, reduce repulsive protein−protein interactions, and promote an overall higher surface affinity and coverage on the mineral. Although it is well known that the acidic groups of statherin are important in controlling HAP growth, these studies suggest a role for the basic groups in the function of statherin and in its adherence to the mineral surface.

ACKNOWLEDGMENT

We thank Professor Wim G. J. Hol and Dr. Thomas R. Hinds for kindly permitting the use of their isothermal titration microcalorimeter. We acknowledge Dr. Allison Campbell from the Pacific Northwest National Laboratory for providing us with the hydroxyapatite samples. We also thank Dr. Martin Sadilek for help with mass spectrometry analysis of the proteins and Mr. Robert Britschgi for help with protein synthesis and purification.

SUPPORTING INFORMATION AVAILABLE

REDOR dephasing curves and $T_{1\rho}$ data for statherin and mutants adsorbed onto HAP. This material is available free of charge via the Internet at http://pubs.acs.org.

REFERENCES

1. Schlesinger, D. H., and Hay, D. I. (1977) Complete covalent structure of statherin, a tyrosine-rich acidic peptide which inhibits calcium phosphate precipitation from human parotid saliva, *J. Biol. Chem. 252*, 1689−1695.
2. Hay, D. I., Smith, D. J., Schluckebier, S. K., and Moreno, E. C. (1984) Relationship between concentration of human salivary statherin and inhibition of calcium phosphate precipitation in stimulated human parotid saliva, *J. Dent. Res. 63*, 857−863.
3. Schlesinger, D. H., Hay, D. I., and Levine, M. J. (1989) Complete primary structure of statherin, a potent inhibitor of calcium phosphate precipitation, from the saliva of the monkey, *Macaca arctoides*, *Int. J. Pept. Protein Res. 34*, 374−380.
4. Johnsson, M., Richardson, C. F., Bergey, E. J., Levine, M. J., and Nancollas, G. H. (1991) The effects of human salivary cystatins and statherin on hydroxyapatite crystallization, *Arch. Oral Biol. 36*, 631−636.
5. Raj, P. A., Johnsson, M., Levine, M. J., and Nancollas, G. H. (1992) Salivary statherin. Dependence on sequence, charge, hydrogen bonding potency, and helical conformation for adsorption to hydroxyapatite and inhibition of mineralization, *J. Biol. Chem. 267*, 5968−5976.
6. Schwartz, S. S., Hay, D. I., and Schluckebier, S. K. (1992) Inhibition of calcium phosphate precipitation by human salivary statherin: structure-activity relationships, *Calcif. Tissue Int. 50*, 511−517.
7. Gururaja, T. L., and Levine, M. J. (1996) Solid-phase synthesis and characterization of human salivary statherin: a tyrosine-rich phosphoprotein inhibitor of calcium phosphate precipitation, *Pept. Res. 9*, 283−289.

8. Douglas, W. H., Reeh, E. S., Ramasubbu, N., Raj, P. A., Bhandary, K. K., and Levine, M. J. (1991) Statherin: A major boundary lubricant of human saliva, *Biochem. Biophys. Res. Commun. 180*, 91−97.
9. Hahn Berg, I. C., Lindh, L., and Arnebrant, T. (2004) Intraoral lubrication of PRP-1, statherin and mucin as studied by AFM, *Biofouling 20*, 65−70.
10. Amano, A., Sharma, A., Lee, J. Y., Sojar, H. T., Raj, P. A., and Genco, R. J. (1996) Structural domains of *Porphyromonas gingivalis* recombinant fimbrillin that mediate binding to salivary proline-rich protein and statherin, *Infect. Immun. 64*, 1631−1637.
11. Nagata, H., Sharma, A., Sojar, H. T., Amano, A., Levine, M. J., and Genco, R. J. (1997) Role of the carboxyl-terminal region of *Porphyromonas gingivalis* fimbrillin in binding to salivary proteins, *Infect. Immun. 65*, 422−427.
12. Contucci, A. M., Inzitari, R., Agostino, S., Vitali, A., Fiorita, A., Cabras, T., Scarano, E., and Messana, I. (2005) Statherin levels in saliva of patients with precancerous and cancerous lesions of the oral cavity: a preliminary report, *Oral Dis. 11*, 95−99.
13. Wikiel, K., Burke, E. M., Perich, J. W., Reynolds, E. C., and Nancollas, G. H. (1994) Hydroxyapatite mineralization and demineralization in the presence of synthetic phosphorylated pentapeptides, *Arch. Oral Biol. 39*, 715−721.
14. Long, J. R., Dindot, J. L., Zebroski, H., Kiihne, S., Clark, R. H., Campbell, A. A., Stayton, P. S., and Drobny, G. P. (1998) A peptide that inhibits hydroxyapatite growth is in an extended conformation on the crystal surface, *Proc. Natl. Acad. Sci. U.S.A. 95*, 12083−12087.
15. Shaw, W. J., Long, J. R., Dindot, J. L., Campbell, A. A., Stayton, P. S., and Gary, P. Drobny. (2000) Determination of statherin N-terminal peptide conformation on hydroxyapatite crystals, *J. Am. Chem. Soc. 122*, 1709−1716.
16. Shaw, W. J., Long, J. R., Campbell, A. A., Stayton, P. S., and Gary, P. Drobny. (2000) A solid state NMR study of dynamics in a hydrated salivary peptide adsorbed to hydroxyapatite, *J. Am. Chem. Soc. 122*, 7118−7119.
17. Long, J. R., Shaw, W. J., Stayton, P. S., and Drobny, G. P. (2001) Structure and dynamics of hydrated statherin on hydroxyapatite as determined by solid-state NMR, *Biochemistry 40*, 15451−15455.
18. Gibson, J. M., Raghunathan, V., Popham, J. M., Stayton, P. S., and Drobny, G. P. (2005) A REDOR NMR study of a phosphorylated statherin fragment bound to hydroxyapatite crystals, *J. Am. Chem. Soc. 127*, 9350−9351.
19. Raghunathan, V., Gibson, J. M., Goobes, G., Popham, J. M., Louie, E. A., Stayton, P. S., and Drobny, G. P. (2006) Homonuclear and heteronuclear NMR studies of a statherin fragment bound to hydroxyapatite crystals, *J. Phys. Chem. B 110*, 9324−9332.
20. Goobes, G., Goobes, R., Schueler-Furman, O., Baker, D. B., Stayton, P. S., and Drobny, G. P. (2006) Folding of the C-terminal bacterial binding domain in statherin upon adsorption onto hydroxyapatite crystals, *Proc. Natl. Acad. Sci. U.S.A. 103*, 16083−16088.
21. Hoang, Q. Q., Sicheri, F., Howard, A. J., and Yang, D. S. (2003) Bone recognition mechanism of porcine osteocalcin from crystal structure, *Nature 425*, 977−980.
22. Goobes, R., Goobes, G., Campbell, C. T., and Stayton, P. S. (2006) Thermodynamics of statherin adsorption onto hydroxyapatite, *Biochemistry 45*, 5576−5586.
23. Gullion, T., and Schaefer, J. (1989) Detection of weak heteronuclear dipolar coupling by rotational-echo double-resonance nuclear magnetic resonance, *Adv. Magn. Reson. 13*, 57−83.
24. Gullion, T., and Schaefer, J. (1989) Rotational-echo double-resonance NMR, *J. Magn. Reson. 81*, 196−200.
25. Herzfeld, J., and Berger, A. E. (1980) Sideband intensities in NMR spectra of samples spinning at the magic angle, *J. Chem. Phys. 73*, 6021−6030.
26. Schaefer, J., Stejskal, E. O., and Buchdahl, R. (1977) Magic-angle ^{13}C NMR analysis of motion in solid glassy polymers, *Macromolecules 10*, 384−405.
27. Ebrahimpour, A., Johnsson, M., Richardson, C. F., and Nancollas, G. H. (1993) The characterization of hydroxyapatite preparations, *J. Colloid. Interface Sci. 159*, 158−163.
28. Bjellqvist, B., Hughes, G. J., Pasquali, C., Paquet, N., Ravier, F., Sanchez, J. C., Frutiger, S., and Hochstrasser, D. F. (1993) The focusing positions of polypeptides in immobilized pH gradients can be predicted from their amino acid sequences, *Electrophoresis 14*, 1023−1031.
29. Olsson, D. M., and Nelson, L. S. (1975) Nelder-Mead simplex procedure for function minimization, *Technometrics 17*, 45−51.
30. Duncan, T. M. (1997) *Chemical Shift Tensors*, 2nd ed., The Farragut Press, Madison, WI.
31. Jensen, J. L., Lamkin, M. S., Troxler, R. F., and Oppenheim, F. G. (1991) Multiple forms of statherin in human salivary secretions, *Arch. Oral Biol. 36*, 529−534.
32. Sabatini, L. M., He, Y.-Z., and Azen, E. A. (1990) Structure and sequence determination of the gene encoding human salivary statherin, *Gene 89*, 245−251.
33. Hay, D. I. (1973) The isolation from human parotid saliva of a tyrosine-rich acidic peptide which exhibits high affinity for hydroxyapatite surfaces, *Arch. Oral Biol. 18*, 1531−1540.
34. Li, J., Helmerhorst, E. J., Yao, Y., Nunn, M. E., Troxler, R. F., and Oppenheim, F. G. (2004) Statherin is an in vivo pellicle constituent: identification and immuno-quantification, *Arch. Oral Biol. 49*, 379−385.

BI602345A